IMPROVING COMBUSTION INTENSITY AND MODULATING FLAME BEHAVIORS USING HELICAL-GROOVED CONES

S. C. Yen * **C. L. Shih**

Department of Mechanical and Mechatronic Engineering
National Taiwan Ocean University
Keelung, Taiwan 20224, R.O.C.

ABSTRACT

Four helical-grooved cones were installed behind an unconfined combustion nozzle to increase the bluff-body effect and turbulence intensity (*T.I.*). The cone configurations included a smooth cone and the other three cones cut with 1, 2 and 3 helical v-grooves. Experimental results showed that the helical v-grooves transformed the axial momentum (or the axial velocity) to the angular momentum (or the angular velocity). The *T.I.* was enhanced by increasing the tangential component of fuel-jet momentum. The direct photography and thermocouple were utilized to observe the flame structures and to delineate the characteristic flame modes, flame length, temperature distribution, and combustion intensity. The flame modes were classified as jet flame, flickering flame, bubble flame, recirculation flame, lifted flame and ring flame. The flame length decreases as the groove number increases. The increased *T.I.* and groove number (or bluff-body effect) improve the fuel-air mixing. The total combustion intensity increases with annular-air jet and with the groove number.

Keywords: Helical-grooved cone, Flame length, Combustion intensity.

1. INTRODUCTION

The swirl-jet flow or bluff body were utilized to improve the combustion intensity in the industrial community. The industrial burner and gas turbine utilized the swirl-jet flow and bluff body to create a relative low-pressure zone (or recirculation zone) near the nozzle exit. These two mechanisms increase the diffusion effect between the central and annular jets. The central and annular jets mix intensively due to the increased turbulence intensity (*T.I.*) and flow residence time. Consequently, the combustion stability improves and the blow-off in combusted flame decreases. Rose [1], Chigier and Beer [2], Davies and Beer [3], and Gupta *et al.* [4] investigated the factors of velocity vector and pressure distribution on the combustion efficiency and gas-mixing ratio.

The bluff-body wake occurs in the local low-pressure zone behind the blunt bodies. The back pressure causes the flow behind the bluff body to move in a direction opposite to the main stream flow. A bluff disc was also used to induce the bluff-body effect. The studies on the bluff disc have been classified as the unconfined jet (Chigier and Beer [2]; Davies and Beer [3]; and Li and Tankin [5]) and confined jet (Winterfeld [6]; Calvert [7]; and Taylor and Whitelaw [8]). A study of diffusion flame behind the bluff body by Marsi and Bilger [9] showed that the flame appears to divide into unpenetrated, transitional and penetrated zones. Schefer *et al.* [10] indicated that, in the combustion recirculation zone, the central jet cannot move through the recirculation bubbles due to the low concentration in the high combusted recirculation zone. They also reported that the turbulent fluctuation of axial stress was about two-fold higher than those of the radial and tangential stresses in the recirculation zone near the stagnation point. Additionally, Schefer *et al.* analyzed the axial and radial velocities; and they found that the probability density function is sinusoidal. The sinusoidal probability density function also showed that a large scale periodic flame structure occurs downstream. Roquemore *et al.* [11] also found that the large pseudo-periodic structure occurs downstream and the frequency decreases as the flow moves downstream. Huang and Lin [12] utilized a bluff disc to classify the flame as recirculated, transition, unsteady detached, laminar ring, developing, split flashing and lifted flame modes. The lifted-flame mode shows the characteristics of diffusion flame. In Li and Tankin [5], a study of recirculation-bubble length in cold and thermal flow fields showed that that the recirculation-bubble length in the attached flame mode is half the length observed in the cold flow.

The first theoretical studies of swirl jet phenomena, which were performed by Loitsyanskii [13] and Gortler [14] in the 1950s, tested the simplified boundary-layer equation. Devices used experimentally to produce swirl flow include the rotating cylinder (Rose [1],

* Corresponding author (scyen@mail.ntou.edu.tw)

DOI : 10.1017/jmech.2012.134
Copyright © 2013 The Society of Theoretical and Applied Mechanics, R.O.C.
https://doi.org/10.1017/jmech.2012.134 Published online by Cambridge University Press

Hartnett and Eckert [15], and Lay [16]), tangential swirl generator (Chigier and Beer [2], and Chigier and Chervinsky [17]), and vane guider (Kerr and Fraser [18], and Cheng *et al.* [19]). Chervinsky [20] also experimentally studied the swirl-intensity effect on the flame width, flame length, temperature distribution and mass entrainment. He found that the swirl intensity correlates positively with the flame width, maximum temperature, and mass entrainment for each test condition. He also found that the increased swirl intensity shortens the flame length due to the increased turbulent fluctuation. Chen *et al.* [21] determined that a four-way stagnation point occurs at the top end of the recirculation zone. Therefore, this four-way point increases turbulence intensity and mixing efficiency, which then stabilizes the combustion flame.

The bluff body and swirl mechanism have been widely utilized to increases the turbulence intensity. This study was motivated to utilize the both mechanisms to increase *T.I.* In order to save the energy consumption, this study utilized the passive device by combining the bluff-body cone and helical v-grooves milled on the cones. Namely, this study utilized the helical-grooved cones to increase the effects of bluff body and turbulence intensity. The helical-grooved cone was installed near the outlet of a central-fuel jet. These helical v-grooves transform the axial-flow momentum to tangential-flow momentum. The increased tangential momentum then raised *T.I.* in the flame field. The mixing of air and fuel was therefore increased. Finally, the effects of increased *T.I.* on flame characteristics, temperature distribution and the combustion intensity were also included. The direct photography and thermocouple were utilized to observe and analyze the characteristic flame mode, flame length, temperature distribution, and combustion intensity. Finally, the qualitative analysis was performed to present the performance trend influenced by the *T.I.* or groove rifles.

2. EXPERIMENTAL ARRANGEMENTS

2.1 Experimental Setup

This investigation utilized the helical v-grooved cones to increase the combustion intensity. Figure 1 schematically shows the arrangement of experimental equipments (San and Hsu [22]). The annular air-jet was driven by a centrifugal blower, and an acoustical filter installed behind the blower was utilized to remove the high-frequency noises. Moreover, the central fuel-jet exhaled from the fuel tank was ignited behind the nozzle. The flame modes and combustion intensity were then observed and analyzed. The honeycombs and screen filter were placed upstream to stabilize the fuel and air flows. The experimental apparatus included four components: The noise filter, settling chamber, helical v-grooved cones and flame-monitor sections. In the noise-filter section, the honeycombs and stainless-steel meshes were used to reduce the flow noise. The honeycombs reduced the radial-direction noise, and the meshes eliminated the axial-direction

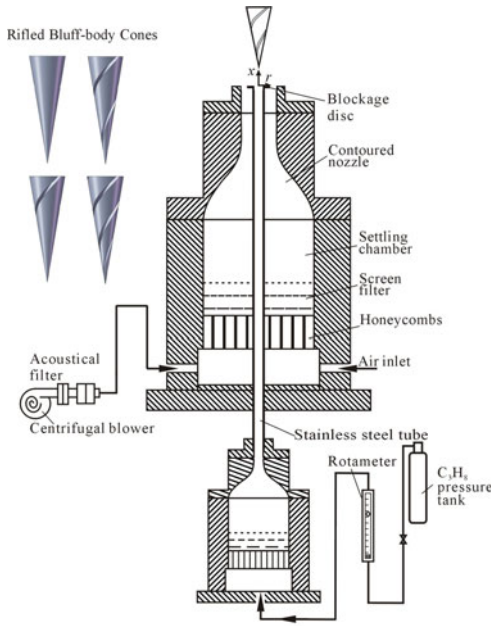


Fig. 1 Experimental setup

noise. The settling chamber reduced the *T.I.* of upstream free-stream. Specifically, the helical v-grooved cones was installed outside the nozzle to increase the *T.I.* The effects of helical v-grooved cones on flame behaviors, temperature distribution and combustion intensity were studied. In the flame-monitor section, the exit diameter of annular air-jet (D_o) was 30mm, and the outlet diameter of central fuel-jet (d) was 5mm. A bluff disc (diameter = 20cm) was installed along the central axis of helical v-grooved cones. The x-r coordinate defined the characteristic positions observed in this investigation, where x represents the axial and r denotes the radial directions. Additionally, the fuel used in this study was commercial propane (95% C_3H_8, 3.5% C_2H_6 and 1.5% C_4H_{10}).

2.2 Helical V-Grooved Cone

The bluff-body cone was supported by two slender L-type stainless-steel rods. These thin stainless steel rods (diameter = 0.45mm) were fixed on the bluff disc. Additionally, the Reynolds number based on the steel-rod diameter was maintained below 77 to prevent vortex shedding behind the thin rod. The bluff-body cone was supported by two slender stainless-steel rods. The smooth cones (height = 30mm and bottom diameter = 10mm) were made of bronze and were milled by a machine center. For the other three helical-grooved cones, the dimensions of v-groove are 1.85 and 1.2mm in depth and width, respectively. Furthermore, the effect of groove number on flow behaviors was tested by milling the smooth cones with 1, 2, and 3 helical v-grooves.

2.3 Turbulence Intensity Anemometry

The turbulence intensity was obtained from the velocity fields measured using a hot-wire probe (TSI 1220-PI2.5). The highest temperature at which the

https://doi.org/10.1017/jmech.2012.134 Published online by Cambridge University Press

hot-wire probe can operate was 300°C. The diameter and length of hot-wire were 5μm and 1.5mm, respectively, and the dynamic response frequency is 15kHz ~ 25kHz. Figure 2 shows the distribution of *T.I.* versus the annular-jet velocity (u_a) for a fixed central-jet velocity (u_c) of 2m/s. For a 3-grooved cone, the *T.I.* is 10.6 when u_a = 2.5m/s, which is about 4 times higher than the *T.I.* of 2.6 observed when u_a = 0m/s. Figure 2 also shows that turbulence intensity increases with the number of helical grooves. At u_a = 2.5m/s, the *T.I.* of 10.6 observed behind a 3-grooved cone is approximately 45.2% higher than the *T.I.* of 7.3 observed behind a smooth cone.

2.4 Temperature Measurements

The temperature distribution is related to the combustion intensity. Therefore, an R-type thermocouple (Pt-Pt/13% Rh, Ω Limited) was utilized to obtain the time-averaged temperature distributions. The thermocouple-wire diameter of 125μm corresponds to an approximate response frequency of 13Hz (referencing the Ω Handbook 2000). The probed signals were also obtained with a West data logger (Model P8010$^+$). Additionally, the average temperature was calculated using 30-second period of recorded temperature signals.

2.5 Flame Photography

The flame patterns and flame lengths were visualized directly using a Nikon CCD recorder (Model D70s) with the resolution of 3008 × 2000 pixels and the exposure time of 30 – 1/8000s. The direct color-photography was utilized to identify the flame phenomena and flame lengths. The flame lengths were measured by the traditional photography method. Then, the flame lengths was calculated by averaging 10 taken photos with an exposure time of 10 seconds for each photo.

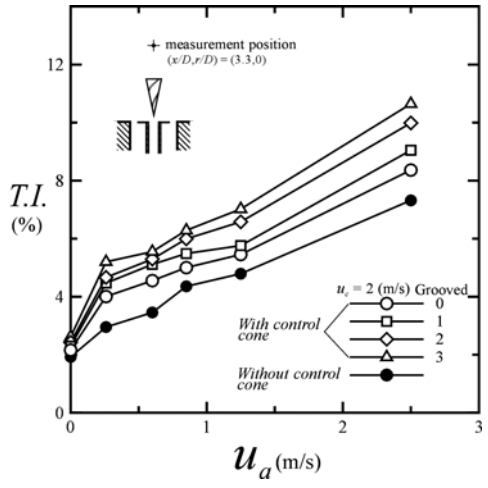


Fig. 2 Distribution of turbulence intensity (*T.I.*) versus the annular-jet velocity (u_a) for a fixed central-jet velocity (u_c) of 2m/s

2.6 Experimental Uncertainty

The flow rate of air and commercial propane were measured using the rotameters. The accuracy of rotameter is ±1% of full scale calibrated with a micro-flow calibration system. The experimental measurement of flame length utilized the direct photo visualization by using a line gauge (ruler). Therefore, the measurement uncertainty is approximately < 0.5%. The uncertainty of the turbulence intensity measurement is within 1.6%. The highest-temperature positions were measured by using an *x-y-z* stage. The measurement uncertainty is approximately < 0.5% in this investigation. Furthermore, the temperatures in the flame field were measured by a data logger (Model P8010$^+$, West Corp.) and an R-type thermocouple (Pt-Pt/13% Rh, Ω Limited). The error of R-type thermocouple is ±1.5°C (handbook, Ω Limited).

3. RESULTS AND DISCUSSION

3.1 Flame Behaviors and Characteristic Flame Patterns

Flame behaviors. Figure 3 shows the near-field flame patterns behind the smooth (non-grooved) cones. A Nikon CCD camera (Model D70s, resolution = 3008 × 2000 pixels, exposure time = 30 – 1/8000s) was utilized to record the flame behaviors. The color photographs were then used to characterize the flame patterns. In Figs. 3(a) ~ 3(f), the velocity of the central fuel jet (u_c) is 2m/s. In Figs. 3(g) ~ 3(l), the velocity of the central fuel jet is 5m/s. Furthermore, the velocities of annular air jet (u_a) are varied. The previous study [23,24] shows that the flame phenomena include the jet flame, flickering flame, and lifted flame.

Figure 3(a) shows that the blue flame occurs at x/D < 0.5 and that yellow flame occurs downstream while u_a = 0m/s. The flame behavior is characterized as a laminar diffusion flame, and the flame pattern is jet-flame mode. In Fig. 3(b), the flame behaviors resemble those in Fig. 3(a) where u_a = 0.26m/s. Figure 3(c) reveals that the bud-like flame occurs downstream and

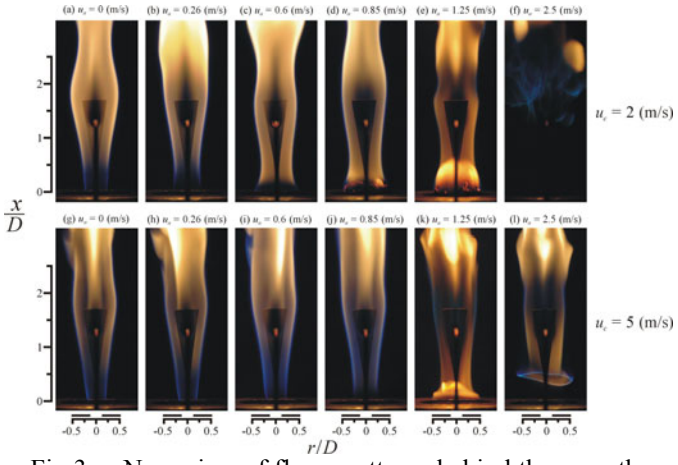


Fig.3 Near view of flame patterns behind the smooth /non-grooved cone. (a) ~ (f): u_c = 2; and (g) ~ (l): u_c = 5m/s. Shutter speed = 1/2000 seconds

https://doi.org/10.1017/jmech.2012.134 Published online by Cambridge University Press

that the blue flame occurs near the fuel exit as u_a = 0.6m/s. This blue flame broadens laterally and the increased annular air jet destabilizes the flame flickering. This flickering flame indicates the phenomenon of flame transition. Therefore, this flame is called the flickering flame mode. Figure 3(d) delineates that the bubble flame occurs near the fuel exit (at about x/D = 0.25) when u_a = 0.85m/s. The blue flame near the fuel exit gradually changes to a yellow flame as u_a increases. Additionally, the soot moves inside the bubble and some soot is deposited on the exit disc. This flame is designated the bubble flame mode. As u_a increases to 1.25m/s, Fig. 3(e) shows that recirculation occurs at x/D < 0.5. The flame near the fuel exit turns from blue to yellow due to the high annular-jet velocity. Furthermore, few soot moves around the flame field and some soot deposit on the bluff disc due to the high annular-jet velocity entraining the less air into the recirculation zone. This flame mode is called the recirculation flame mode. Figure 3(f) shows that the flame base is lifted away from the bluff disc at u_a = 2.5m/s. The blue flame occurs at x/D = 1.2 − 2.2. Moreover, the yellow flame occurs downstream and moves chaotically. The high annular-jet velocity produces highly unstable flame structures. This flame mode is called lifted flame mode. Additionally, the recirculation and lifted flame modes shows the characteristics of turbulent diffusion flame and the eddies that occur around the flame.

Figures 3(g) and 3(h) show that the blue flame occurs near the bluff disc whereas the yellow flame occurs downstream, respectively. This flame is called the jet flame mode (*i.e.*, similar to the flame modes shown in Figs. 3(a) and 3(b)). Figures 3(i) and 3(j) show that the flame flickers unstably due to the increased annular jet flow. Consequently, this flame is called the flickering flame mode (as shown in Fig. 3(c)). Figure 3(k) shows that the high annular-jet velocity induces the recirculation. This flame mode is therefore designated the recirculation flame mode. Additionally, the recirculation height in Fig. 3(k) is shorter than that in Fig. 3(e) because the high central-jet velocity restrains the recirculation. As u_a increases to 2.5m/s, Fig. 3(l) reveals that the blue ring flame is stable at x/D = 0.5 and that the recirculation zone extends downstream. This flame mode is called the ring-flame mode.

Characteristic flame patterns. Figure 4 shows the distribution of the characteristic flame patterns with varying u_a and u_c. The characteristic flame phenomena include the jet-flame, flickering flame, bubble flame, recirculation flame, ring flame and lifted flame (as shown in Fig. 3). The lifted-flame mode occurs at low u_c and high u_a. In the previous studies, the flame phenomena shows the phenomena of jet, flickering and lift flame without the existence of bluff cone. In Fig. 4, near the mode divisions for separating the different flame modes, the measured velocity induces some uncertainties. The uncertainties of u_a and u_c are about ±0.1m/s and ±0.2m/s, respectively. The jet-flame mode occurs at low u_a, and the effect of u_c on jet-flame mode is weak. Additionally, the lifted flame mode occurs in the high u_a-low u_c regime. Furthermore, the ring-flame mode occurs at high u_a and u_c.

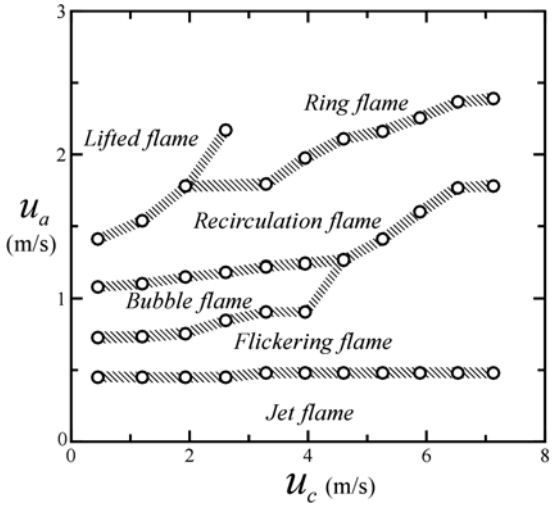


Fig. 4 Distribution of characteristic flame modes

3.2 Flame Length

The flame lengths for each condition were determined by averaging 10 photos taken using a CCD camera (Nikon Model D70s, exposure time = 10 second). Figure 5 reveals the photographs of the far-field flames for measuring the full flame length at u_c = 2m/s and varying u_a. Furthermore, the effect of number of helical grooves on flame length were also considered. Figures 5(a-1) ~ 5(a-6) show the flame photographs around the smooth cone. These figures reveal that the flame length decreases as u_a increases. Moreover, comparisons of flame length around the 1-grooved cone (Figs. 5(b-1) ~ 5(b-6)), 2-grooved cone (Figs. 5(c-1) ~ 5(c-6)), and 3-grooved cone (Figs. 5(d-1) ~ 5(d-6)) show that flame length decreases as the number of helical grooves increases.

Figure 6 depicts the distributions of non-dimensional flame length (H_f / D) versus u_a while u_c = 2 and 5m/s by testing the effect these four bluff-body cones. At u_c = 2m/s, the increased annular air flow is entrained in the flame base and then broaden the flame configuration. Therefore, the flame length is shortened in the lifted flame mode due to the occurrence of high-turbulent diffusion flame. Specifically, the shortest flame length occurs in the 3-grooved cone, and the non-dimensional flame length of 7.2 at u_a = 2.5m/s (*T.I.* = 10.6%) is about 50% shorter than the flame length of 14.4 observed at u_a = 0m/s (*T.I.* = 2.6%) when u_c = 2m/s. Furthermore, for a 3-grooved cone and u_c = 5m/s, the H_f / D of 10.8 observed when u_a = 2.5m/s is about 41% shorter than the H_f / D of 18.3 observed when u_a = 0m/s.

3.3 Temperature Distributions

Figure 7 shows the radial-temperature distributions (T) at various axial positions for u_a = 0m/s (jet flame mode) and 2.5m/s (lifted flame mode) where u_c is fixed at 2m/s. Moreover, the effects of number of helical grooves on temperature distribution are also considered. Figures 7(a) and 7(d) display the radial-temperature

https://doi.org/10.1017/jmech.2012.134 Published online by Cambridge University Press

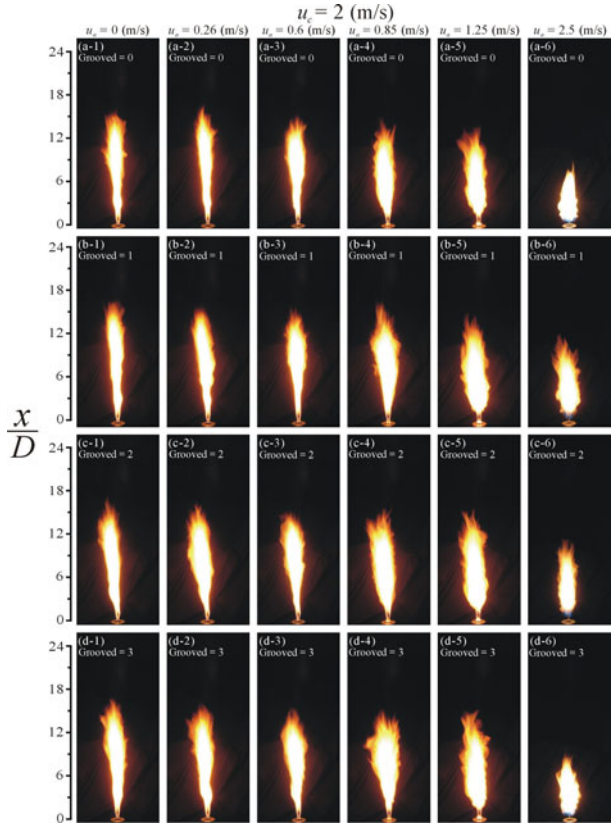


Fig. 5 Far view of flame patterns behind the bluff-body cones. (a-1) ~ (a-6): smooth; (b-1) ~ (b-6): 1-grooved; (c-1) ~ (c-6): 2-grooved; and (d-1) ~ (d-6): 3-grooved. u_c = 2m/s and shutter speed = 10 seconds

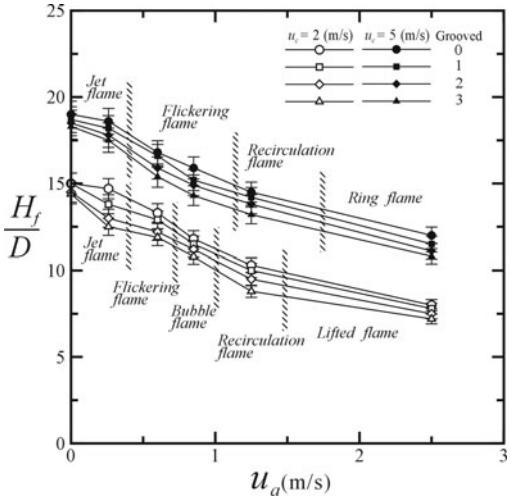


Fig. 6 Variations of normalized flame height (H_f /D) against u_a

distribution around a smooth cone where u_a = 0 and u_a = 2.5m/s, respectively. Figures 7(a) and 7(d) show the jet-flame mode and lifted-flame mode, respectively. In Fig. 7(a), where u_a = 0m/s (*T.I.* = 2.1%), the highest temperature (1585K) occurs at x/D = 1.0, and the lowest temperature (930K) occurs along the axial axis at x/D = 3.75. Moreover, in Fig. 7(d), for u_a = 2.5m/s (*T.I.* = 8.3%), the highest temperature (1496K) occurs at x/D = 3.75 along the axial axis.

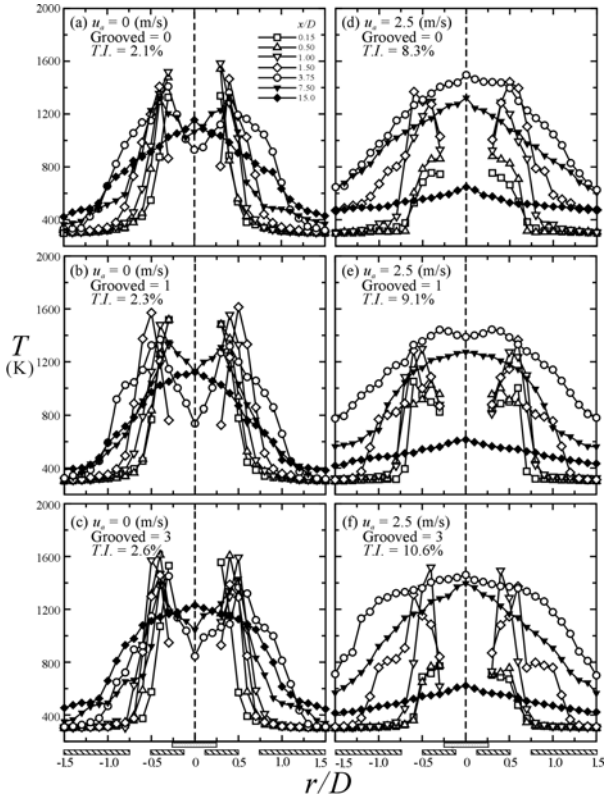


Fig. 7 Radial-temperature distributions along x-direction at various axial positions. u_c = 2m/s

Figures 7(b) and 7(e) show the radial temperature distributions for a 1-grooved cone where u_a = 0m/s (*T.I.* = 2.3%) and u_a = 2.5m/s (*T.I.* = 9.1%), respectively. Moreover, Figs. 7(c) and 7(f) show the temperature distributions around the 3-grooved cone where u_a = 0m/s (*T.I.* = 2.6%) and u_a = 2.5m/s (*T.I.* = 10.6%), respectively. The increase in annular-jet velocity significantly changes the radial-temperature distributions. Moreover, the increased helical v-grooves broaden the temperature distribution behind the helical v-grooved cones. Namely, the increased turbulence intensity (or number of helical v-groves) and bluff-body effect improve the mixing efficiency.

Figure 8 shows the curves of non-dimensional position (L_f / D) against u_a for the smooth cone and helical v-grooved cones where L_f is the axial position of the highest temperature for each flame condition. In Fig. 8, the central fuel velocity is fixed at 2m/s, and the annular air velocity is varied. Figure 8 shows that L_f /D decreases as u_a increases. Specifically, at high u_a, the effects of bluff-body cone decrease the L_f /D more significant than that of a conventional nozzle. In Fig. 8, the L_f /D of 11 for a 3-grooved cone (*T.I.* = 2.6%) is approximately 14% shorter than the L_f /D of 12.8 (without the effect of bluff-body cone, *T.I.* = 0.08%) where u_a = 0m/s. Furthermore, when u_a increases to 2.5m/s, the L_f /D of 3.0 for a 3-grooved cone (*T.I.* = 10.6%) is about 64% shorter than 8.25 for a conventional nozzle (*T.I.* = 0.11%). Conclusively, the bluff-body cone and helical v-grooves increase the turbulence intensity. Then, the highest temperature positions descend toward the nozzle exit and the flame lengths shortened (as shown in Fig. 6).

https://doi.org/10.1017/jmech.2012.134 Published online by Cambridge University Press

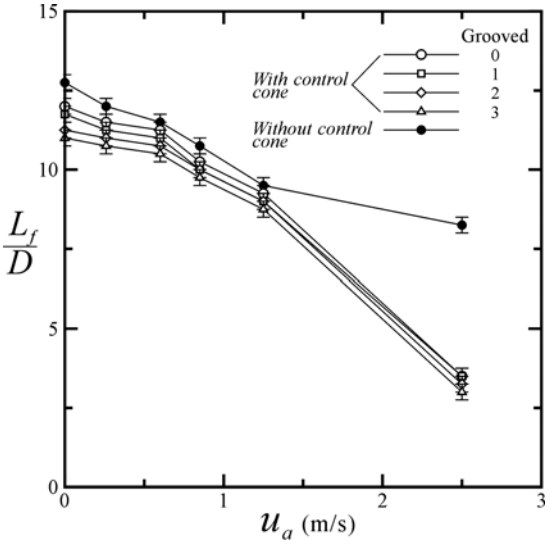


Fig. 8 Variations of non-dimensional position (L_f/D) against u_a where L_f is the axial position of the highest temperature. u_c = 2m/s

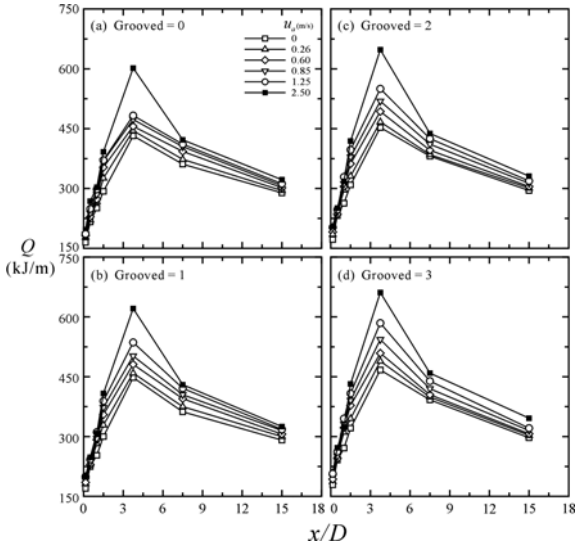


Fig. 9 Variations of combustion intensity (Q) versus x/D behind u_c = 2m/s

3.4 Combustion Intensity

The thermal effect of adding a helical v-grooved cone is determined using the combustion intensity (Q) defined in Eq. (1) (Huang and Yen [25]; Yen [26]):

$$Q = \int \rho \cdot C_p \cdot T \cdot 2\pi r \cdot dr \tag{1}$$

where T is the temperature distribution along the r axis on a specific plane, ρ denotes the air density, and C_p represents the specific heat of air at constant pressure. The relationship of C_p and T was formulated as C_p = 0.97 + (6.8 × 10^{-5}) × T + (1.65 × 10^{-7}) × T^2 − (5.67 × 10^{-8}) × T^3kJ/kg·K (Cengel and Boles [27]). The value of ρ is determined by T using the ideal gas equation. The velocity profiles for each particle in the flame field are difficult to measure. Consequently, this investigation uses the same velocity for the various burned gases to simplify the calculation of Q.

Figure 9 delineates the distributions of combustion intensity as a function of non-dimensional axial coordinates where u_c = 2.0m/s. Figure 9 shows that Q increases with u_a behind the smooth cone. Moreover, Q increases with x/D when x/D < 3.75 and then decreases as x/D increases when x/D > 3.75 (behind a four-way saddle point). Figure 9(a) shows that the maximum Q of 602kJ/m occurs at x/D = 3.75 behind the smooth cone where u_a = 2.5m/s ($T.I.$ = 8.3%). Namely, the maximum Q occurs in the lifted-flame mode for smooth cone. At high annular air velocity, the fuel and oxygen have not enough reaction time to complete the combustion process. Therefore, the flame was lifted away the nozzle exit and occurred over the nozzle exit. The drawn-in air was not consumed near the flame-air interface. Specifically, the air was joined into the fuel jet. Namely, the premixed air-fuel flow occurs in the lifted-flame mode of a non-premixed combustion. Moreover, the yellow flame was changed to blue flame and the temperature (combustion intensity) was lifted. Figures 9(b) ~ 9(d) show that the maximum Q values are 621, 648 and 661kJ/m for 1-, 2-, and 3-grooved cone, respectively.

In order to determine the integral combustion effect of smooth/grooved cones, the total combustion intensity (Q_{tot}) is utilized and defined in Eq. 2:

$$Q_{tot} = \int_0^{15} Q \cdot d\left(\frac{x}{D}\right) \tag{2}$$

Figure 10 depicts the variations of Q_{tot} against u_a where u_c = 2m/s behind the smooth/grooved cones. In Fig. 10, the Q_{tot} increases with u_a, and furthermore, the increase of number of helical v-grooves promotes the Q_{tot}. Additionally, Fig. 10 shows that the Q_{tot} of 16.1 MJ for a 3-grooved cone ($T.I.$ = 10.6%) is about 8% higher than Q_{tot} of 14.9 MJ in a smooth cone ($T.I.$ = 8.3%) where u_a = 2.5m/s. For a 3-grooved cone, Fig. 10 also shows that the Q_{tot} is 16.1 MJ at u_a = 2.5m/s ($T.I.$ = 10.6%), which is approximately 21% higher than the Q_{tot} of 13.3 MJ at u_a = 0m/s ($T.I.$ = 2.6%).

4. CONCLUSIONS

In this investigation, four smooth/grooved cones were utilized to increase the (total) combustion intensity. The helical v-grooves increased the turbulence intensity and then increased the mixing efficiency. These smooth/grooved cones were placed along the axial axis and near the exit of central-fuel jet. The measurement and observation schemes utilized in this study included the direct photography and temperature-detected thermocouple. After determining temperature, (total) combustion intensity can be found. The following conclusions are drawn from the results and discussions.

1. Six flame modes — jet-flame, flickering-flame, bubble flame, recirculation flame, ring flame and lifted flame — are defined using various annular air-jet and central fuel-jet velocities.

https://doi.org/10.1017/jmech.2012.134 Published online by Cambridge University Press

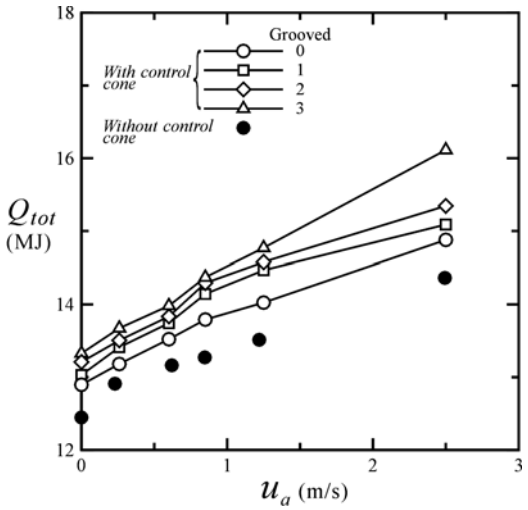


Fig. 10 Variations of total combustion intensity (Q_{tot}) versus u_a while u_c = 2m/s

2. Flame length deceases as the number of helical v-grooves increases and flame length shortens as annular air velocity increases.
3. The increase in annular-jet velocity and the number of helical v-grooves broadens the radial-temperature distributions where x/D < 3.75. Namely, the increases in turbulence intensity (or number of helical v-grooves) and bluff-body effect improves the mixing efficiency.
4. The total combustion intensity (Q_{tot}) increases with u_a and with the number of helical v-grooves. In the current study, the Q_{tot} of 16.1MJ obtained when u_a = 2.5m/s ($T.I.$ = 10.6%) is approximately 21% higher than the Q_{tot} of 13.3MJ obtained when u_a = 0m/s ($T.I.$ = 2.6%).

ACKNOWLEDGMENTS

This research was supported by the National Science Council of the Republic of China, under Grant No. NSC 98-2221-E-019-040-MY3.

NOMENCLATURES

A_a exit area of annular air jet: $\pi(D_o^2-D^2)/4$, 392.7mm^2
A_c exit area of central fuel jet: $\pi d^2/4$, 19.6mm^2
D diameter of blockage disc, 20mm
d exit diameter of central fuel jet, 5mm
D_o outer diameter of annular air jet at exit, 30mm
Q combustion intensity
Q_a volumetric flow rate of annular air flow
Q_c volumetric flow rate of central fuel flow
Q_{tot} total combustion intensity
r radial coordinate, originated at center of blockage disc
x axial coordinate, originated at center of blockage disc
u_a volumetric mean axial velocity of annular air jet at exit: Q_a / A_a
u_c volumetric mean velocity of central fuel jet at exit: Q_c / A_c

REFERENCES

1. Rose, W. G., "A Swirling Round Turbulent Jet 1-Mean-flow Measurements," *Journal of Applied Mechanics*, **29**, pp. 615–625 (1962).
2. Chigier, N. A. and Beer, J. M., "Velocity and Static Pressure Distributions in Swirling Air Jets Issuing from Annular and Divergent Nozzles," *Journal of Fluids Engineering*, ASME, **86**, pp. 788–798 (1964).
3. Davies, T. W. and Beer, J. M., "Flow in the Wake of Bluff-body Flame Stabilizers," *Proceedings Twentieth Symposium (International) on Combustion*, The Combustion Institute, pp. 631–638 (1971).
4. Gupta, A. K., Lilley, D. G. and Syred, N., *Swirl Flow*, Abacus Press, Cambridge, pp. 1–293 (1984).
5. Li, X. and Takin, R. S., "A Study of Cold and Combusting Flow around Bluff-body Combustors," *Combustion Science and Technology*, **52**, pp. 173–206 (1987).
6. Winterfeld, G., "On Process of Turbulent Exchange Behind Flame Holders," *Tenth Symposium (International) on Combustion*, The Combustion Institute, pp. 1265–1273 (1965).
7. Calvert, J. R., "Experiments on the Low-speed Flow Past Cones," *Journal of Applied Mechanics*, **27**, pp. 273–289 (1967).
8. Taylor, M. K. P. and Whitelaw, J. H., "Velocity Characteristics in the Turbulent Near Wakes of Confined Axisymmetric Bluff Bodies," *Journal of Applied Mechanics*, **139**, pp. 391–416 (1984).
9. Marsri, A. R. and Bilger, R. W., "Turbulent Diffusion Flame of Hydrocarbon Fuel Stabilized on a Bluff Body," *Proceedings Twentieth Symposium (International) on Combustion*, The Combustion Institute, pp. 319–326 (1984).
10. Schefer, R. W., Namazian, M. and Kelly, J., "Velocity Measurement in Turbulent Bluff-body Stabilized Flows," *AIAA Journal*, **32**, pp. 1844–1851 (1994).
11. Roquemore, W. M., Tankin, R. S., Chiu, H. H. and Lottes, S. A., "A Study of a Bluff-body Combustor Using Laser Sheet Lighting," *Experiments in Fluids*, **4**, pp. 205–213 (1986).
12. Huang, R. F. and Lin, C. L., "Characteristic Modes and Thermal Structure of Nonpremixed Circular-Disc Stabilized Flames," *Combustion Science and Technology*, **100**, pp. 123–139 (1994).
13. Loitsyanskii, L. G., "The Propagation of a Twisted Jet in an Unbounded Space Filed with the Same Fluid," *Prikladnaya Matematica I Mekhanika*, **17**,

https://doi.org/10.1017/jmech.2012.134 Published online by Cambridge University Press

pp. 3–6 (1953).
14. Gortler, H., "Decay of Swirl in an Axially Symmetrical Jet far from the Orifice," *Revista Matematica Hispano American*, Series 4, **14**, pp.143–178 (1954).
15. Hartnett, J. P. and Eckert, E. R. G., "Experiment Study of the Velocity and Temperature Distribution in a high Velocity Vortex Type Flow," *Journal of Fluids Engineering*, *Transactions of the ASME*, Series D, **79**, pp. 751–757 (1957).
16. Lay, J. E., "An Experiment and Analytical Study of the Vortex-flow Temperature Separation by Position of Spiral and Axial Flows," *Journal of Fluids Engineering*, *Transactions of the ASME*, Series D, **81**, pp. 202–212 (1959).
17. Chigier, N. A. and Chervinsky, A., "Experimental Investigation of Swirling Vortex Motions in Jets," *Journal of Applied Mechanics*, **89**, pp. 443–451 (1967).
18. Kerr, N. M. and Fraser, D., "Swirl Part 1: Effect on Axisymmetrical Turbulent Jets," *Journal of Institute Fuel*, **38**, pp. 519–526 (1965).
19. Cheng, T. S., Chao, Y. C., Wu, D. C., Yuan, T., Lu, C. C., Cheng, C. K. and Chang, J. M., "Effects of Fuel-air Mixing on Flame Structures and NOx Emissions in Swirling Methane Jet Flames," *Proceedings Twenty-Seventh Symposium (International) on Combustion*, The Combustion Institute, pp. 1229–1237 (1998).
20. Chervinsky, A., "Turbulent Swirling Jet Diffusion Flames," *AIAA Journal*, **7**, pp. 1877–1883 (1969).
21. Chen, R. H., Driscoll, J. F., Kelly, J., Namazian, M. and Schefer, R. W., "A Comparison of Bluff-body and Swirl-stabilized Flame," *Combustion Science and Technology*, **71**, pp. 197–217 (1990).
22. San, K. C. and Hsu, H. J., "Characteristics of Flow and Flame Behavior behind Rifled/Unrifled Nozzles," *Journal of Engineering for Gas Turbines and Power*, **131**, p. 051501 (2009).
23. Chung, S. H. and Lee, B. J., "On the Characteristics of Laminar Lifted Flames in a Nonpremixed Jet," *Combustion and Flame*, **86**, pp. 62–72 (1991).
24. Lee, K. M., Kim, T. K., Kim, W. J., Kim, S. G., Park, J. and Keel, S. I., "A Visual Study on Flame Behavior in Tone-Excited Non-Premixed Jet Flames," *Fuel*, **81**, pp. 2249–2255 (2002).
25. Huang, R. F. and Yen, S. C., "Aerodynamic Characteristics and Thermal Structure of Nonpremixed Reacting Swirling Wakes at Low Reynolds Numbers," *Combustion and Flame*, **155**, pp. 539–556 (2008).
26. Yen, S. C., "Flow Control and Flame Manipulation of Swirling Jets Using a Dual- Disc Blockage Configuration," Ph.D. Dissertation, National Taiwan University of Science and Technology, Taipei, Taiwan, pp. 63–65 (2003).
27. Cengel, Y. A. and Boles, M. A., *Thermodynamics: An Engineering Approach*, Third Edition, McGraw-Hill, p. 901 (1998).

(Manuscript received February 20, 2012,
accepted for publication June 21, 2012.)

https://doi.org/10.1017/jmech.2012.134 Published online by Cambridge University Press